STEWARD. 1027

PREPRINTS

of the

STEWARD OBSERVATORY

THE UNIVERSITY OF ARIZONA
TUCSON, ARIZONA 85721 U.S.A.

No. 1027

FERMILAB
JAN 1 8 1992
LIBRARY

No ADS
No HEP

THE CASE FOR A TIME DEPENDENT QUANTIZED REDSHIFT

ROUTE TO

NAME	LOCATION

RETURN TO FERMILAB LIBRARY

W. G. Tifft

Steward Observatory
University of Arizona
Tucson, Arizona 85721

Submitted to the Astrophysical Journal.

The Case for a Time Dependent Quantized Redshift

W. G. Tifft
Steward Observatory, University of Arizona
Tucson, Arizona 85721

Abstract

Second epoch 21 cm observations on standard galaxies obtained with the 140 foot telescope confirm that redshift changes appear to have occurred; a pattern of differences which correlate with global redshift phase is present. The period at which the correlations appear was previously predicted as were essentially all other parameters in the analysis. An investigation of 300 foot telescope 21 cm data extending over 10 years has been used to develop and further test a model for the way the variation occurs. Redshifts appear to be relatively stable for intervals of several years and then shift relatively rapidly by multiples of a basic period near 2.7 km s^{-1}. The trend of change is generally down in redshift so that over time a negatively displaced wing appears in redshift residuals. The most recent 140 foot telescope observations indicate that such a shift is apparently developing in the new data. Both 21 cm profile width and shape are parameters in the proposed model for redshift variation. Longer term monitoring promises to provide a very fundamental test on the nature of the redshift

1. INTRODUCTION

Several basic investigations of 21 cm redshifts have recently been carried out (Tifft & Cocke (1988 henceforth TC), Tifft & Huchtmeier (1990 henceforth TH) and Tifft (1990, 1991a,b 1992 henceforth Papers I-IV). The earlier papers contain modern data with an emphasis on high precision; comparisons at the level of a fraction of a km s^{-1} are readily achieved. The later series of papers establishes a system of 21 cm standard objects and examines for intersystem and time dependent effects using the new data and various older studies. Paper III, in particular, developes the concept that the redshift exhibits rapid variability. The phenomenon is intimately related to global redshift quantization. Time dependent deviations are periodic and proportional to the time intervals involved, which appears to rule out most ordinary explanations. The objective of this paper is to develop the evidence for, and the character of, the time dependent changes in the redshift. We draw upon new 21 cm data obtained in 1991 at the National Radio Astronomy Observatory[1] 140 foot (43m) telescope, and we make specific comparisons with data from the Fisher-Tully (1981 henceforth FT) redshift catalog.

The background which led to the time-dependent redshift concept was presented in Paper III and will not be repeated here. Paper III also specifies a number of critical parameters and properties which we shall briefly review. Little or no further flexibility exists with respect to these conditions; they were specified prior to obtaining the 1991 21 cm data presented in this paper. Paper III also preceeded the greater part of the investigations of the FT data contained in this paper. The study of the FT data at profile widths greater than 100 km s^{-1}, contained in this paper, was precipitated as a result of the May 1991 observational findings.

Paper III specifies the solar motion and relativistic correction required for calculating the global quantization phase. The solar motion components assumed are $\theta = 232.2$, $\pi = -36.5$, $Z = 1.2$. The new relativistic correction formalization with $q_o = 0.5$ is assumed; the actual value of q_o is of little importance.

It has been clear since the earliest global studies that quantization properties depend upon 21 cm profile width, W. Paper III defines several important profile width intervals. Two ranges, 50 to 75 km s^{-1}, and 100 to 200 km s^{-1} are recognized as 'critical' windows where properties appear to be stable and especially clear. The narrowest profile galaxies, and objects with profiles between 75 and 100 km s^{-1} wide, are considered to be 'transition' objects. The principal transition region, W = 75-100 km s^{-1}, is readily associated with the transition from dwarf irregular galaxies to spirals with a rotating disk. For galaxies with profile widths greater than 200 km s^{-1}, the available data are more limited and the accuracy is lower. Beyond some general comparisons we will not discuss wide profile galaxies in this paper. As was the case for solar motion and relativistic corrections, the profile width windows utilized are defined by prior discussion.

Paper III also provides the basic period(s) for the current analysis. Periodicities in a time dependent situation differ somewhat from the static situation originally considered when global quantization was discovered. In the original form the period was determined to maximize clustering of redshift phase. As discussed in Paper III, if redshift is drifting differentially, maximum phase clumping will not in general yield the true period. A two dimensional analysis is required where redshift phase is plotted against the redshift difference at two epochs. The period is found to optimize 'drift-line' structure in such two dimensional diagrams. The periodic structure seen will depend upon the epochs chosen and the nature of the time drift process. An attempt to define the drift process is one objective of this paper.

As was the case for the original global quantization work, the key objects used to define the period are the narrow profile dwarf galaxies, especially those in the critical width window around W = 60 km s^{-1}. The critical sub-period found in Paper III is 2.6657 km s^{-1}, as shown in Figure 11 of Paper III. This period appears to define a basic interval, but all cycles of this period are not equivalent in their time drift properties. This interval appears to be modulated such that specific higher multiples produce strong periodic patterns. This is, we believe, the origin of the longer periods which have been discussed in past studies. The non-equivalence of different cycles of the 2.6657 km s^{-1} period is well illustrated in Figure 10 of Paper III where the period 5.3313 km s^{-1}, twice 2.6657 km s^{-1}, is utilized. These are the two periods we will use in this paper, which contains, in section 4, a further analysis of the W = 60 km s^{-1} FT sample. The four to

[1] The National Radio Astronomy Observatory is operated by Associated Universities, Inc., under contract with the National Science Foundation.

five significant figure accuracy of the periods arises from the fact that they are fine tuned over more than 1000 cycles of the 2.6657 km s^{-1} period.

Since Paper III utilized the narrow critical window data to fine tune the period and solar motion, the narrow window data cannot be used to directly evaluate the significance of the periodicity in the data set. In paper III evaluations of significance were largely confined to working with higher multiples of the 2.6657 km s^{-1}interval. In section 5 of this paper we will demonstrate the significance of this interval in the second critical window centered around W = 150 km s^{-1}.

The final parameter, which we will use to distinguish subsamples, is the 21 cm profile shape or asymmetry index A. The precedent has been set in previous papers and is illustrated in Paper III. We will generally broadly distinguish up to three classes, distinctly negative A, near symmetrical, and distinctly positive A. The index A, formally defined in TC, is a measure of the deviation of the profile midpoint by area from the midpoint defined by profile level-crossings. Profiles with negative A are dominant on the high redshift side, those with positive A show a low redshift dominant profile.

Section 2 presents the new 1991 NRAO 140 foot telescope data. Section 3 compares the May 1991 data with the 1988 definition observations of the 21 cm standard objects. The time dependent pattern found in this internal comparison provides the point of departure to examine a longer baseline interval, back to the 1970's using FT data, done in sections 4 and 5. Section 6 illustrates continued trends seen in October 1991 140 foot data. Discussion in section 7 includes specific predictions for future work.

2. 1991 OBSERVATIONS

The objective of the TC and TH 21 cm investigations was to determine the precision obtainable through a study of internal and external comparisons. The first indications of a possible redshift time dependence became apparent during these studies. The work culminated with the establishment of a set of 100 standard objects defined in Paper I. Investigations of radial and temporal effects in Papers II and III indicated a need to continue observations of the standards. The first major reobservations took place between May 3-14 and October 19-24, 1991. The observations were made at the NRAO 140 foot telescope using the L-band receiver. Procedures used duplicated the original observations in nearly all respects. Total power mode was employed using the original set of positions and center velocities. Bandwidths were set at 10, 5, or 2.5 MHz, as done in 1988, according to the profile width. A few objects were observed at two bandwidths. The only change in procedure was to replace 1.25 MHz observations, used for the narrowest profiles in 1988, with 2.5 MHz observations. The reason for this change is discussed in Paper I, and concerns possible slight systematic effects on flux determinations. Regular pointing and flux calibration observations were made using standard continuum sources. Pointing deviations rarely exceed 10 arc seconds. Flux data are not presented here; no significant improvement over the 1988 data is possible at this time. A second set of galaxies emphasizing objects with wider profiles, where the standard set is deficient, was also observed. Discussion of this sample will be deferred to a later date.

Table 1 contains the May 1991 observations. TC, FT, and UGC numbers are serial identification numbers from the original TC analysis, the Fisher-Tully (1981) catalog, and the Uppsala General Catalog (Nilson 1973). FT numbers beginning with zero, or greater than 1171, are NGC numbers. A complete description of the notation is given in TC or Paper I. The fourth column lists the bandwidth used; 2.5 MHz is abbreviated as 2. Columns V_h, W, A, and S/N list the heliocentric redshifts, profile widths at 20% of the average height of the central 80% of the profile area, the asymmetry index, and the signal-to-noise figure. Definitions of these quantities are given in TC and Paper I. The column Q contains comment codes defined in notes appended to the table. The final columns, DV and DW, give the difference in V_h and W, from the 1988 data, in the sense (new−old) = (1991−1988). Table 2 contains the October 1991 observations in a format identical to Table 1 except that all comments are appended to Table 1.

Table 1

May 1991 Data

TC	FT	UGC	BW MHz	V_h km s^{-1}	W km s^{-1}	A	S/N	Q	DV km s^{-1}	DW km s^{-1}
6	0	192	5	−347.3	88.3	−1.10	99.4		0.9	1.3
6	0	192	2	−347.4	87.2	−1.11	145.3		0.8	0.2
7	62	300	2	...	...	...	...	XF	...	...
432	80	0	2	1073.5	103.0	−1.03	32.8		0.3	−0.2
11	0	668	2	−232.4	38.2	−1.01	250.7		0.1	0.2
906	0598	1117	5	−181.1	171.9	−1.17	195.4	M33	−0.2	−0.2
18	96	1149	2	657.6	75.1	1.07	121.4		−0.1	−0.5
443	100	1201	2	...	...	...	...	XS	...	...
23	118	1501	2	198.5	124.6	1.23	19.4	S	1.3	2.1
454	127	1831	2	...	...	...	...	XS	...	...
36	145	2034	2	576.7	65.7	−1.13	26.0	S	−0.5	−1.2
459	150	2080	2	...	...	...	...	XS	...	...
460	151	2082	2	...	...	...	...	XS	...	...
41	162	2193	2	517.6	43.1	−1.02	63.2	S	0.4	0.7
43	168	2302	2	1103.5	70.8	−1.10	26.2	S	0.5	0.9
46	183	0	2	...	...	...	...	XF	...	...
468	190	0	2	...	...	...	...	XS	...	...
473	206	2729	10	1937.7	264.5	1.14	11.0	S!	−2.7	−7.1
48	231	2855	10	1216.4	466.6	1.23	18.9	S!	1.9	−6.9
51	238	2953	10	893.7	496.5	1.11	10.3	RS	−1.8	3.5
477	242	3013	10	2459.1	349.8	1.03	10.8	S!	−2.1	−3.3
481	248	3137	5	995.3	253.3	1.14	13.5	S	2.2	3.2
482	251	3144	5	1636.9	162.4	−1.13	18.0	S	0.1	2.0
56	252	3174	5	670.2	122.1	1.17	13.7	S	−0.5	−3.8
486	271	3273	5	617.7	207.6	−1.02	15.6	S	1.8	2.5
487	277	3303	5	519.3	178.4	−1.03	12.6	S!	0.3	5.1
61	0	3334	10	3930.7	695.0	−1.45	9.5	S	0.7	−38.1
64	0	3384	2	1089.8	92.7	−1.08	19.9	S	0.6	1.0
492	302	0	10	731.8	328.8	−1.11	23.1	S	0.5	1.6
70	306	3475	5	486.2	180.2	1.02	19.7	S	0.1	−6.0
71	307	3496	2	1593.9	118.4	1.08	2.9	FS!	6.4	29.8
74	314	3574	5	1441.4	170.3	−1.07	17.3	S	0.5	6.1
499	320	3685	2	1796.2	100.1	−1.10	26.5		−0.1	−1.7
81	322	3711	5	433.3	173.2	1.08	27.1	RS	−0.6	−3.3
83	325	3809	10	2200.7	476.7	1.06	12.6		−3.2	−5.5
87	331	3851	2	100.6	115.1	1.00	61.5		0.7	−0.9
93	338	3974	2	273.4	89.5	−1.05	34.5		0.8	0.7
100	351	4305	5	156.7	73.6	1.03	156.6	+C	0.0	0.2
100	Comp	0	5	−145.8	38.3	−1.12	47.7	cmp	...	...
100	351	4305	2	156.7	73.5	1.03	112.1		0.0	0.1

Table 1—*Continued*

TC	FT	UGC	BW MHz	V_h km s^{-1}	W km s^{-1}	A	S/N	Q	DV km s^{-1}	DW km s^{-1}
106	0	4483	2	156.8	53.7	1.10	19.4		0.0	−0.8
117	406	5139	2	139.8	46.8	1.01	27.5		−0.7	−0.8
122	0	5251	10	1480.8	302.2	−1.27	18.6		0.7	−6.1
124	0	5280	10	1538.5	300.1	−1.15	6.7	FS!	10.9	10.2
128	431	5373	2	301.2	64.8	1.06	35.8		0.0	1.0
134	450	0	2	324.1	65.3	1.02	96.8	+C	−0.2	−0.3
134	Comp	0	2	133.4	47.3	−1.13	16.2	cmp	...	...
136	456	5557	5	592.7	150.2	1.13	26.4		−0.7	2.5
143	485	5829	2	629.8	96.9	1.06	21.8		0.1	−1.0
150	507	6079	5	683.5	249.2	−1.05	20.9		0.7	1.0
917	3556	6225	10	698.1	337.1	1.01	25.7		−0.4	3.9
917	3556	6225	5	699.1	334.3	1.01	17.9		0.6	1.1
164	536	6360	5	1153.9	129.8	−1.17	17.6		−0.8	−1.8
175	565	6628	2	848.8	56.0	−1.07	17.4		−0.8	−0.8
182	589	6817	2	241.1	72.1	−1.12	25.3		−0.4	1.7
188	628	7047	2	206.4	87.0	−1.26	16.7		0.8	2.8
201	675	7278	2	292.4	90.7	1.07	84.1		−0.1	−1.4
210	706	7534	2	723.7	77.7	1.08	18.9		0.4	4.7
217	715	7577	2	199.9	59.7	1.26	18.1	+C	4.4	7.0
217	Comp	0	2	274.8	68.7	−1.03	6.4	cmp	...	...
239	770	7907	5	640.0	192.7	−1.14	60.6	C	0.2	−4.4
259	826	0	5	740.6	133.0	−1.22	23.0		−0.3	1.3
260	834	8188	2	321.9	59.1	1.11	26.5		0.7	2.7
273	863	8320	2	192.1	87.5	1.05	24.7		1.0	−0.1
295	933	8837	2	139.7	109.0	1.21	9.1		−1.3	1.1
302	944	8981	5	231.4	200.6	−1.31	205.8	M101	1.1	−0.3
304	947	9013	5	274.3	56.3	1.01	70.4	C	−0.5	−0.1
304	947	9013	2	274.3	56.1	1.00	76.6	+C	−0.5	−0.3
304	Comp	0	2	168.3	96.0	...	2.8	Gau	...	...
308	966	9240	2	149.9	66.2	−1.17	12.4		−0.3	−5.8
322	999	0	5	1841.5	172.5	1.00	9.2		1.8	−15.5
328	0	9797	10	3398.8	387.1	−1.13	11.5		8.5	16.5
555	1019	9801	10	667.9	501.6	−1.28	20.6		−0.8	2.1
559	1027	9906	10	655.1	214.2	1.08	17.4		−0.7	−0.4
333	1028	9912	2	1031.0	57.3	−1.07	11.3		−0.4	−6.7
338	1035	10014	5	1121.7	132.8	1.04	12.8		1.2	0.4
562	1042	10075	10	834.4	321.9	1.24	22.4		2.0	1.0
345	1046	10310	2	716.6	103.9	1.04	8.5		−0.4	−5.7
565	1048	10359	5	907.7	234.3	1.00	24.9		−0.6	1.8
347	0	10445	5	962.2	169.8	−1.04	11.7		−2.2	−4.5

Table 1—*Continued*

TC	FT	UGC	BW MHz	V_h km s^{-1}	W km s^{-1}	A	S/N	Q	DV km s^{-1}	DW km s^{-1}
353	1056	10736	5	491.1	160.7	−1.14	11.1		−0.1	1.3
354	1058	10792	2	1234.1	75.0	1.08	6.5		1.2	−0.2
358	0	10897	5	1322.6	143.7	1.09	10.9	S	2.2	5.2
364	1074	11193	5	1511.4	120.4	−1.19	4.0	FS	−1.7	−3.4
932	6643	11218	10	1485.7	381.2	−1.07	10.6		0.1	21.9
365	1075	11220	2	1448.0	97.0	1.03	9.3		0.3	7.3
583	1078	11300	5	490.8	228.1	−1.06	13.3		0.8	0.4
372	−11	0	2	−78.9	42.2	1.03	22.5		0.0	4.9
373	−15	0	2	1561.9	98.5	1.06	19.2		−0.9	5.5
374	−12	0	2	−56.9	85.9	...	256.2	Gau	−0.1	0.7
377	1082	0	2	1423.5	92.1	1.22	9.8		−0.9	−3.7
379	0	11604	10	1424.6	343.6	−1.10	8.2		2.9	5.5
380	1085	0	2	−141.4	34.8	−1.09	12.1		0.5	−3.2
605	1088	11707	5	904.9	206.5	1.20	19.3	S	...	...
387	0	11759	5	3258.1	151.8	−1.58	7.6	S	−1.7	−9.5
609	1093	11861	10	1481.2	273.5	1.05	12.3		−0.4	10.5
393	1098	11891	5	460.8	154.3	1.29	20.6	r	−1.0	−1.9
396	1107	0	2	...	...	...	...	XF	...	...
399	1113	12082	2	803.5	86.9	−1.13	18.0		0.8	0.8
402	1117	12113	10	816.9	535.6	−1.11	8.4	S	−0.8	−0.8
620	1139	12392	2	...	...	...	...	S	...	...
936	7640	12554	10	371.6	268.8	−1.13	30.2	r	0.2	−0.2
412	1147	12613	2	−186.6	42.0	−1.34	18.0	R	−0.2	0.0
413	1149	12632	5	422.1	127.7	−1.08	19.3	rS	0.3	−0.3
414	1159	12732	5	748.3	137.0	1.14	37.7	S	0.1	−1.9
415	1160	12754	5	748.7	214.3	1.03	14.0	S	−1.8	−0.2
417	0	12894	2	320.7	79.1	−1.59	8.9	S	−2.0	10.4
418	1171	0	2	−122.9	79.7	−1.13	86.1		0.2	−0.6
418	1171	0	2	...	...	...	...	CB	...	...
418	Bcmp	0	2	−185.3	87.1	−1.09	18.2	Bcm	...	...

C = Galaxy has companion, +C = in main beam, <,> indicate below or above
cmp = Second object in main beam, Bcm = Object in West off field
CB = Object in West (CC = East) off field disturbes baseline or profile
Gau = Gauss fit to profile
F = Object too weak for effective measurements
H = Hanning smoothing employed
I = Interference, <,> indicate below or above
R = Ringing, r = minor ringing effects, <,> indicate below or above
S = Baseline disturbed by Sun, S! if effect is large
X = Not measured, XF = Too weak, XS = Solar interference
0VH = Galactic HI disturbes profile

Table 2

October 1991 Data

TC	FT	UGC	BW MHz	V_h km s^{-1}	W km s^{-1}	A	S/N	Q	DV km s^{-1}	DW km s^{-1}
6	0	192	5	−347.6	87.7	−1.13	78.1		0.6	0.7
6	0	192	2	−347.8	87.5	−1.14	141.5		0.4	0.5
7	62	300	2	...	...	...	...	XF	...	...
432	80	0	2	1073.4	102.8	−1.06	47.6		0.2	−0.4
11	0	668	2	−232.4	38.0	−1.02	247.8		0.1	0.0
906	0598	1117	5	−181.8	172.2	−1.14	172.8	M33	−0.9	0.1
18	96	1149	2	658.0	75.4	1.07	115.9		0.3	−0.2
443	100	1201	2	852.7	335.5	−1.12	27.5		0.8	3.0
23	118	1501	2	198.3	123.8	1.21	20.5		1.1	1.3
454	127	1831	2	529.8	481.0	−1.16	16.2		−2.2	−3.0
36	145	2034	2	579.1	62.7	1.02	32.4		1.9	−4.2
459	150	2080	2	904.9	145.1	−1.04	44.1	Su?	1.2	1.5
460	151	2082	2	708.0	216.9	−1.04	15.7		1.6	0.7
41	162	2193	2	518.0	43.5	−1.00	63.8		0.8	1.1
43	168	2302	2	1103.5	71.2	−1.12	39.4	C<?	0.5	1.3
46	183	0	2	...	...	...	...	XF	...	...
468	190	0	2	1710.4	326.7	−1.14	20.2	C>?	2.2	−0.5
473	206	2729	10	1943.8	278.0	1.11	11.3		3.4	6.4
48	231	2855	10	1215.7	481.5	1.16	19.4		1.2	8.0
51	238	2953	10	897.0	494.5	1.10	9.0	R<	1.5	1.5
477	242	3013	10	2458.0	344.2	−1.04	15.4		−3.2	−8.9
481	248	3137	5	990.9	251.1	1.10	9.4		−2.2	1.0
482	251	3144	5	1636.6	160.6	−1.09	12.3		−0.2	0.2
56	252	3174	5	668.4	119.6	1.13	11.4		−2.3	−6.3
486	271	3273	5	618.0	204.9	1.02	16.6		2.1	−0.2
487	277	3303	5	519.0	177.8	−1.03	17.4		0.0	4.5
61	0	3334	10	3925.9	697.9	−1.36	9.1	I>	−4.1	−35.2
64	0	3384	2	1094.5	105.5	1.09	17.2		5.3	13.8
492	302	0	10	733.0	324.7	−1.11	32.0		1.7	−2.5
70	306	3475	5	486.2	182.2	1.03	4.8	R	0.1	−4.0
71	307	3496	2	...	...	...	...	XF	...	...
74	314	3574	5	1442.9	161.3	−1.02	17.9		2.0	−2.9
499	320	3685	2	1796.8	102.3	−1.10	22.4		0.5	0.5
81	322	3711	5	431.6	178.3	1.07	24.2	RH	−2.3	1.8
83	325	3809	10	2200.7	471.3	1.05	13.0		−3.2	−10.9
87	331	3851	2	100.5	115.7	−1.02	69.0		0.6	−0.3
93	338	3974	2	272.8	89.2	−1.09	36.7		0.2	0.4
100	351	4305	5	156.7	73.4	1.03	164.9	+C	0.0	0.0
100	Comp	0	5	−145.5	38.6	−1.07	45.0	cmp	...	...
100	351	4305	2	156.5	73.3	1.03	120.8		−0.2	−0.1

Table 2—*Continued*

TC	FT	UGC	BW MHz	V_h km s^{-1}	W km s^{-1}	A	S/N	Q	DV km s^{-1}	DW km s^{-1}
106	0	4483	2	156.1	56.0	1.06	14.2		−0.7	1.5
117	406	5139	2	141.2	47.1	1.09	26.4		0.7	−0.5
122	0	5251	10	1478.1	304.2	−1.35	19.2		−2.0	−4.1
124	0	5280	10	1545.0	307.9	−1.15	5.1	F	17.4	18.0
128	431	5373	2	301.5	64.4	1.05	53.7		0.3	0.6
134	450	0	2	324.5	65.9	1.04	94.3	+C	0.2	0.3
134	Comp	0	2	132.4	46.4	−1.07	13.5	cmp	...	...
136	456	5557	5	591.3	148.7	1.10	36.3		−2.1	1.0
143	485	5829	2	629.6	101.8	1.07	30.3		−0.1	3.9
150	507	6079	5	681.3	249.3	−1.07	32.4		−1.5	1.1
917	3356	6225	10	...	...	...	...	XS	...	...
917	3556	6225	5	697.9	334.2	−1.00	24.4	S	−0.6	1.0
164	536	6360	5	1154.2	129.4	−1.19	28.4	S	−0.5	−2.2
175	565	6628	2	849.2	56.1	−1.05	32.9		−0.4	−0.7
182	589	6817	2	241.6	70.8	−1.09	39.5		0.1	0.4
188	628	7047	2	205.3	90.2	−1.23	26.7		−0.3	6.0
201	675	7278	2	292.5	92.3	1.06	74.7		0.0	0.2
210	706	7534	2	722.1	74.9	1.04	19.9		−1.2	1.9
217	715	7577	2	197.0	55.4	1.08	28.5	S+C	1.5	2.7
217	Comp	0	2	271.0	68.2	−1.24	9.5	cmp	...	...
239	770	7907	5	639.3	198.1	−1.12	101.8	C	−0.5	1.0
259	826	0	5	...	...	...	...	XS	...	...
260	834	8188	2	321.8	57.0	1.14	36.3		0.6	0.6
273	863	8320	2	190.9	88.6	1.02	38.0	S	−0.2	1.0
295	933	8837	2	140.5	113.1	1.20	13.0	S	−0.5	5.2
302	944	8981	5	230.7	201.7	−1.23	171.3	M101	0.4	0.8
304	947	9013	5	274.5	57.0	−1.01	70.4	C	−0.3	0.6
304	947	9013	2	274.2	56.5	−1.02	84.6	S+C	−0.6	0.1
304	Comp	0	2	167.1	88.5	...	2.7	Gau	...	...
308	966	9240	2	149.9	67.2	−1.13	25.9		−0.3	−4.8
322	999	0	5	...	...	...	...	XS	...	...
328	0	9797	10	...	...	...	...	XS	...	...
555	1019	9801	10	...	...	...	...	XS	...	...
559	1027	9906	10	...	...	...	...	XS	...	...
333	1028	9912	2	1033.2	60.2	1.03	14.0		1.8	−3.8
338	1035	10014	5	...	...	...	...	XS	...	...
562	1042	10075	10	...	...	...	...	XS	...	...
345	1046	10310	2	716.9	107.9	1.03	14.3		−0.1	−1.7
565	1048	10359	5	908.1	235.0	1.05	22.2	S!	−0.2	2.5
347	0	10445	5	961.7	174.1	−1.12	17.2	S!	−2.7	−0.2

Table 2—*Continued*

TC	FT	UGC	BW MHz	V_h km s^{-1}	W km s^{-1}	A	S/N	Q	DV km s^{-1}	DW km s^{-1}
353	1056	10736	5	490.8	160.7	−1.07	12.3	S	−0.4	1.3
354	1058	10792	2	1232.5	72.8	−1.09	9.9		−0.4	−2.4
358	0	10897	5	1318.2	138.2	−1.01	16.8	S!	−2.2	−0.3
364	1074	11193	5	...	...	...	...	XF	...	...
932	6643	11218	10	1481.6	364.1	−1.07	9.2	S!	−4.0	4.8
365	1075	11220	2	1449.9	96.6	1.05	9.1	S	2.2	6.9
583	1078	11300	5	489.1	230.8	−1.04	20.1		−0.9	3.1
372	−11	0	2	−79.3	36.1	1.02	22.0		−0.4	−1.2
373	−15	0	2	1563.6	102.8	1.13	18.7		0.8	9.8
374	−12	0	2	−56.7	79.5	1.03	256.0	0VH	0.1	−5.7
377	1082	0	2	1423.8	93.3	1.22	16.2		−0.6	−2.5
379	0	11604	10	1429.2	348.8	−1.12	14.1		7.5	10.7
380	1085	0	2	−141.0	37.3	−1.02	20.7		0.9	−0.7
605	1088	11707	5	905.6	207.0	1.23	18.0		...	...
387	0	11759	5	3257.3	157.1	−1.71	9.0		−2.5	−4.2
609	1093	11861	10	1479.1	270.1	1.05	19.0	CC?	−2.5	7.1
393	1098	11891	5	461.2	155.3	1.29	22.6	r	−0.6	−0.9
396	1107	0	2	...	...	...	...	XF	...	...
399	1113	12082	2	802.1	87.1	−1.16	25.1		−0.6	1.0
402	1117	12113	10	816.2	533.8	−1.16	17.9	R<	−1.5	−2.6
620	1139	12392	2	1705.9	305.7	1.45	19.8		0.5	−2.1
936	7640	12554	10	372.2	267.9	−1.15	21.3	rR	0.8	−1.1
412	1147	12613	2	−186.5	41.3	−1.32	19.7	CBr	−0.1	−0.7
413	1149	12632	5	422.8	125.1	−1.03	17.3	R<	1.0	−2.9
414	1159	12732	5	748.1	138.5	1.11	30.6		−0.1	−0.4
415	1160	12754	5	750.8	213.1	1.03	16.7		0.3	−1.4
417	0	12894	2	322.8	76.5	−1.51	7.3		0.1	7.8
418	1171	0	2	−122.7	78.7	−1.12	79.2		0.4	−1.6
418	1171	0	2	−120.5	75.4	−1.14	80.9	CB!	2.6	−4.9
418	Bcmp	0	2	−185.4	89.0	−1.12	17.4	Bcm	...	...

3. THE STANDARDS IN MAY 1991

Three years elapsed between the establishment of the 21 cm standards in 1988 and the observations obtained in May 1991. Since FT comparisons, discussed in Paper I, suggest that deviations up to 10

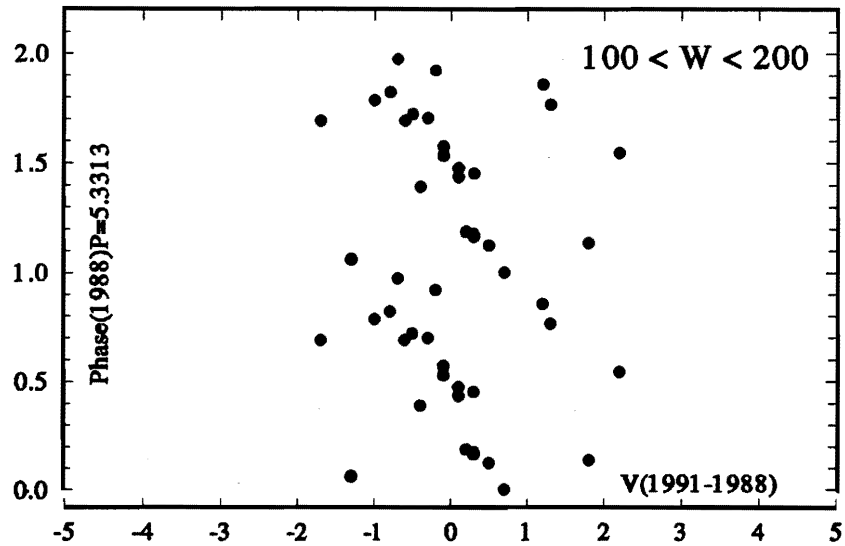

Fig 1. Phase-deviation diagram for the May 1991 140 foot telescope data on galaxies with profiles 100 to 200 km s^{-1} wide and S/N > 10. Phase is calculated for the 5.3313 km s^{-1} period at the epoch of the standard observations, 1988.25, and repeated in a double cycle to facilitate viewing the periodic pattern. Points distribute along sloping lines with a phase offset at zero deviation. The deviation scale is in km s^{-1}.

km s^{-1} can occur over 10-12 years, we would expect visible changes in 3 years. Comparison of the 1988 and 1991 observations appear to confirm this expectation. Figure 1 displays the redshift difference (May 1991 − 1988), for the critical W = 100-200 km s^{-1} window, as a function of global phase at the 5.3313 km s^{-1} period. A double cycle of phase is plotted to facilitate viewing periodic patterns. The points distribute in a sloping pattern, undisplaced from zero near phase 0.25-0.5, and maximally displaced near phase 0.75-0.0. All parameters in this diagram were fixed prior to the 1991 observations. The diagram appears to be consistent with a real phase dependent drift in redshift since normal random error would not be expected to correlate with phase.

To examine the properties of the data in Figure 1 further it is useful to perform a simple transformation. If points are moving in time, the pattern seen will depend upon the epoch at which the phase is calculated. Figure 1 is plotted at epoch 1988.25, the epoch when the standards were defined. If we assume that each point drifts at a uniform rate determined by its present displacement from zero, a point discussed further below, we can reconstruct the diagram at any epoch. In particular we can choose an epoch where linear sloping features become horizontal. This occurs for Figure 1 near 1994.0. Figure 2 shows this transformation for periods of 5.3313 and 2.6657 km s^{-1}; only the phase was advanced in this example; deviations will also change by a corresponding scale factor.

Several properties of the diagram are now readily apparent. There seems little doubt that the points are periodically distributed. There is, however, a distinct phase displacement at zero; positively and negatively displaced points are not continuously related. The phase shift appears to be very close to one half of the 2.6657 km s^{-1} period. Actual mean phases are close to 0.05 and 0.55. No special significance can be attached to a precise value since small solar motion uncertainties, especially in Z, could shift the mean phase slightly. Figure 2 also demonstrates the multiplicity of periods which can fit the data. Periods of 10.6626 and 21.3252 km s^{-1} also show unique patterns. Drift rates appear to vary in a regular pattern over at least four successive 5.3313 km s^{-1} levels. Although we will refer to the 2.6657 km s^{-1} interval as a basic sub-period it should be kept in mind that successive cycles are not equivalent in drift rates, and only some are populated.

Although the continuous simple smooth drift rate model used to generate Figure 2 is useful to illustrate some properties of the data sets, the model is not consistent with observation of discreet levels. Even if we begin with discreet levels, phase wrapping at a wide range of rates should rapidly destroy any semblance of levels. A more likely model is one where specific levels are populated for some significant period of time. Objects then cascade between levels and are seen changing levels only briefly. Such a model will change the

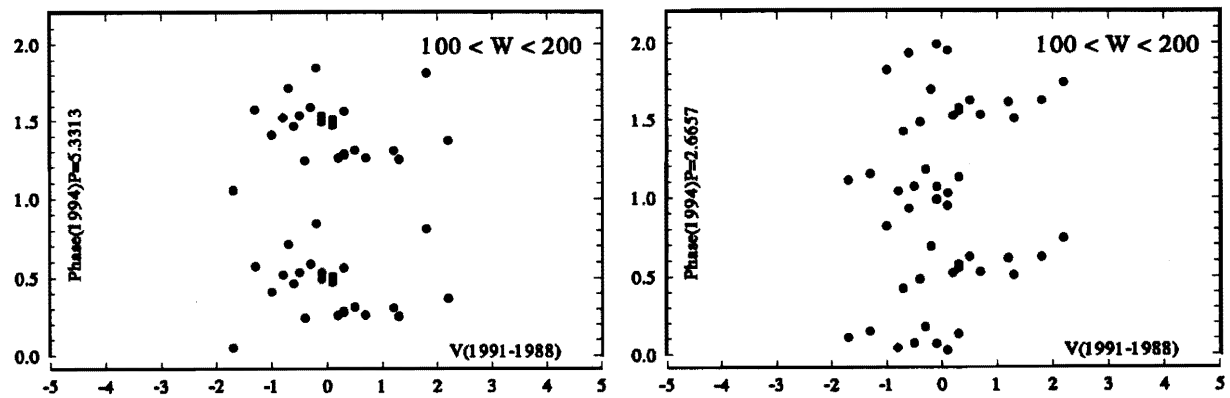

Fig 2. Phase-deviation diagrams for the May 1991 140 foot telescope data on galaxies with profiles 100 to 200 km s^{-1} wide and S/N > 10. The left diagram is the same as Figure 1 with the epoch advanced to 1991 by assuming that phase drift is directly proportional to time. The phase offset at zero deviation is readily seen. The right panel repeats the same data at the 2.6657 km s^{-1} period.

character of Figure 2 slightly. If we imagine looking at such a diagram after a time interval involving several transitions, we might still see horizontal bands, but the the bands will not be continuous, there should be individual clumps separated by the transition intervals. Objects observed in transition should connect the clumps. This is the model we propose. As a first test we will examine the 10-12 year baseline data between TC and FT observations, looking at each of the two critical profile width windows in turn.

4. PROPERTIES OF NARROW PROFILES

300 foot (91m) telescope data for FT galaxies in the W = 50-75 km s^{-1} window were used in Paper III to determine the 2.6657 sub-periodicity and to fine tune the solar motion. We now examine that data from the viewpoint of the interlevel transition model proposed in Section 3. Figure 3 shows the P = 5.3313 km s^{-1} phase-deviation diagram for all TC galaxies with FT data and S/N > 10. Phase is referred to the FT epoch which is characterized as 1975 but can range from 1973 to 1977 for individual points. This diagram differs slightly from the corresponding figure in Paper III where 1988 redshifts were combined with the TC values and a slightly narrower window was used. We opt here to have the maximum possible sample in the minimum time interval. Two arrows in the figure represent transitional paths between phase states which appear as incipient clumps within the levels. The phase 0.5-0.6 level appears to have two states while the phase 0.0 level has only one.

In the integrated form shown in Figure 3 there is little obvious information. To test the level and transition concept we need to divide the sample into homogeneous subsamples which we can associate with different stages. We have only one parameter to use, the profile asymmetry; however, Paper III and earlier studies indicate that asymmetry and phase are often correlated. In this particular case the correlation is quite informative. Figure 4 replots Figure 3 to include only those objects within 5% of being symmetrical. Two of the three clumps noted above, one at each level, now stand out quite clearly. No points appear along a transition connection between the regions although they bear the expected relationship to each other as indicated by the upper vector in Figure 3. From the perspective of the model, the symmetric profile objects can be presumed to be in stable states at the time of each observation; objects in the zero phase group must have changed states *between* the observations.

Figure 5 contains the galaxies with profiles negatively asymmetric beyond the 5% level. The right hand panel contains two circles, which mark the locations of the symmetrical profile objects, and repeats the hypothesized transition vectors from Figure 3. The negative asymmetry points distribute along the transition line and extend past the phase zero clump to end at a second suggested clump near phase 0.6. A dashed region defining this clump is drawn shifted one 5.3313 km s^{-1} cycle from the clump with zero redshift displacement. The negative A objects lie along tracks which *begin* at stationary states; from the perspective

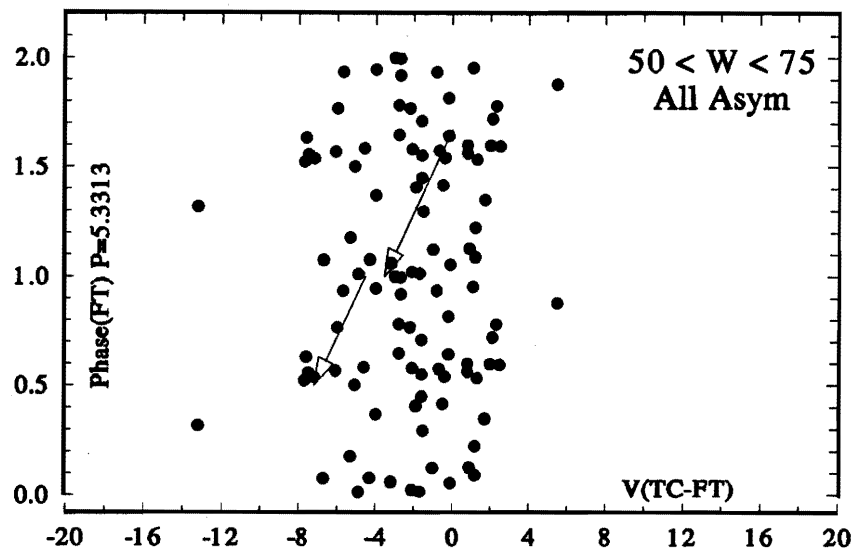

Fig 3. Phase-deviation diagram for TC − FT 300 foot telescope data on galaxies with profiles 50 to 75 km s^{-1} wide and S/N > 10. Phase is calculated for the 5.3313 km s^{-1} period at the FT epoch. The deviation scale is in km s^{-1}. Two vectors illustrate the tracks points would follow if undergoing a transition between levels

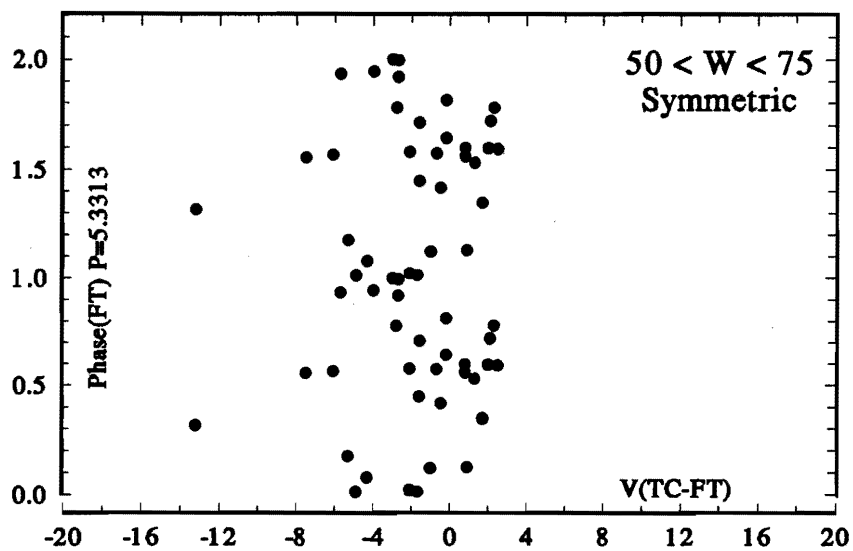

Fig 4. Phase-deviation diagram for TC − FT 300 foot telescope data on galaxies with symmetric profiles 50 to 75 km s^{-1} wide and S/N > 10. The figure is the same as Figure 3 except it omits the galaxies with |A| > 1.04. Two clumps or 'states' are present.

of the model they are consistent with being leading objects in a transition. The 'new' state being formed contains no objects with distinctly positive asymmetry.

Figure 6 contains the galaxies with profiles positively asymmetric beyond the 5% level. These points also lie along a sloped line at the expected transition slope, but the line is anticorrelated in location with the negative asymmetry feature associated with the transition vectors shown. The positive asymmetry feature *ends* at the location of the symmetrical zero phase clump, shown with a circle. The feature extends precisely one periodic cycle and begins in the fuzz to the right of the symmetrical zero phase group. This new region, shown by a dashed circle displaced by one period, contains only positively asymmetric profile objects. From the perspective of the model this region can be interpreted as the last vestige of a previous

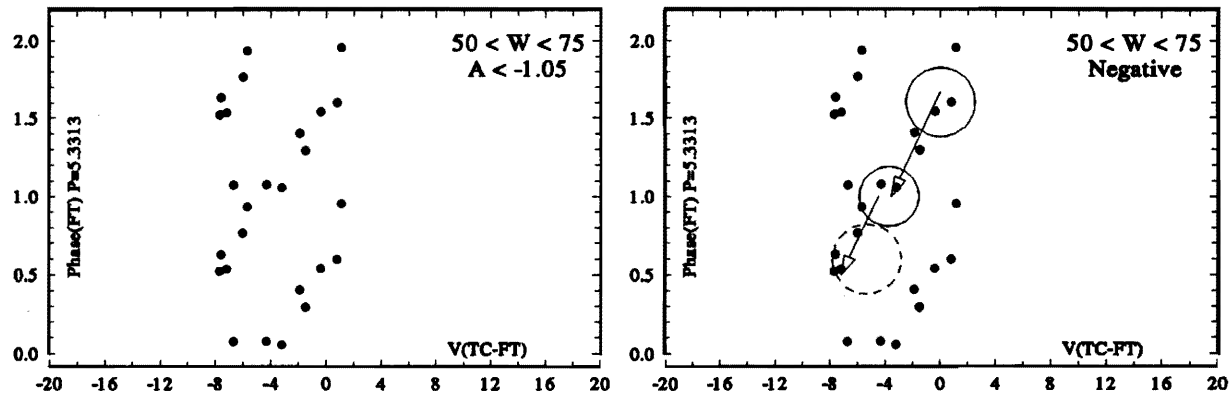

Fig 5. Phase-deviation diagrams for TC – FT 300 foot telescope data on galaxies with negatively asymmetric profiles 50 to 75 km s^{-1} wide and S/N > 10. The figure is the same as Figure 3 except it omits the galaxies with A > −1.05. The right panel repeats the transition vectors from figure 3 and shows the location of the symmetric profile objects with circles. The negatively asymmetric galaxies distribute along transition lines beginning at symmetric regions and end at a dashed region which may just be forming.

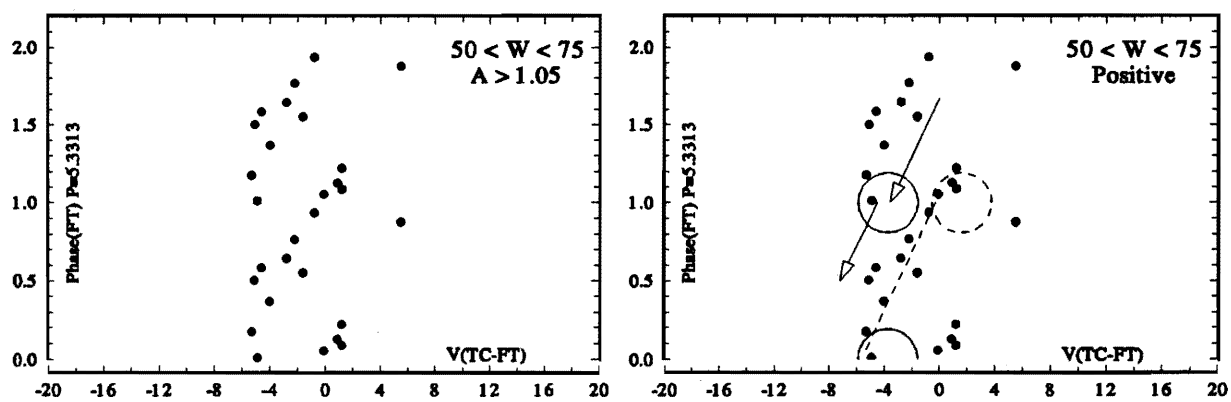

Fig 6. Phase-deviation diagrams for TC – FT 300 foot telescope data on galaxies with positively asymmetric profiles 50 to 75 km s^{-1} wide and S/N > 10. The figure is the same as Figure 3 except it omits the galaxies with A < 1.05. The right panel repeats the transition vectors from figure 3 and shows the location of one of the symmetric profile regions with a circle. The positively asymmetric galaxies distribute along a transition line beginning in a dashed region, which may be a remnant of a former state, and ending at the symmetric region.

state; the positively asymmetric profile objects are consistent with being the last objects to leave a state.

It is essentially impossible to derive meaningful confidence levels for the non-random character of the narrow profile data since they have been used to tune parameters and recognize properties. The data are clearly quite consistent with a level and transition model. The ultimate test of the model in this profile width interval will come soon enough through continued precision monitoring. The principal immediate conclusion we can draw is that asymmetry distinctions provide an important means of defining subsamples.

5. INTERMEDIATE WIDTH PROFILES

Intermediate and wide profile galaxies were recognized, in Paper III, to show time dependent phase and shape correlations. The focus at that time was on the 8 km s^{-1} interval central to the discovery of time dependent changes. The 5.3313 and 2.6657 km s^{-1} periodicities were developed almost entirely in the narrow profile domain. When the May 1991 observations made it clear that the 5.3313 km s^{-1} interval was equally

fundamental in the W = 100-200 km s^{-1} window, the intermediate width profile objects became an obvious testing grounds for the level and transition model. The test is a powerful one since virtually all parameters are fixed and a sizeable sample is available using the 300 foot telescope TC to FT database. As with the narrow profile analysis we omit the more fragmentary 1988 300 foot telescope data to maximize the sample size in as short a recent time interval as possible. The TC observations extended from 1984 to 1986.

The only free parameter is the epoch at which we view the data. Variation of the epoch does not change phase relationships at a fixed redshift deviation, but it does scale deviations and shifts phases. There are two natural choices, the two epochs of observation. From the viewpoint of uncertainties, phase scatter should be minimized by choosing the epoch which has the most accurate redshifts. From the viewpoint of the level and transition model the choice of epoch can affect the appearance of a phase-deviation diagram more significantly. If, at one or both observing epochs, objects are in transition, a transition 'front' may appear as a phase gradient; this is one interpretation of Figure 1. We can scale and rotate this phase line by varying the epoch and assuming a form for the drift as done in Figure 2. In the discussion of the intermediate width TC−FT diagrams which follow we have opted to use an epoch of 1987. The choice of epoch is discussed further in section 6. We assume linear changes with time and epochs of 1975 and 1985 for FT and TC observations. Both deviations and phases are adjusted to the adopted epoch. Under such a transformation the time drift direction is invariant; any displacement in the deviation coordinate produces a corresponding phase shift. Points shift along lines at a fixed slope as epoch is varied.

Figure 7 is the W = 100-200 km s^{-1}, P = 5.3313 km s^{-1}, phase-deviation diagram, epoch 1987, for the TC−FT data with S/N > 10 and A > −1.05. These data are known to show large negative deviations as demonstrated in Paper III. The negative deviations show a distinct periodic structure. The 1987 epoch was chosen because it renders the individual populated levels essentially horizontal, consistent with expected uncertainties. The older FT redshift uncertainty enters the deviation coordinate with nearly full weight while only the newer redshift uncertainty contributes significantly to phase scatter. Figure 7 omits galaxies with significantly negatively asymmetric profiles; these objects are discussed separately below. In the W = 100-200 km s^{-1} window the galaxies with symmetric and positively asymmetric profiles appear to be indistinguishable.

Three drift line vectors are shown in Figure 7. The vectors connect clumps and account for all the significant concentrations as either the starting or ending point of a vector; epoch change affects only the length of a vector, not its orientation or its association with the data points. As with the narrow profile data

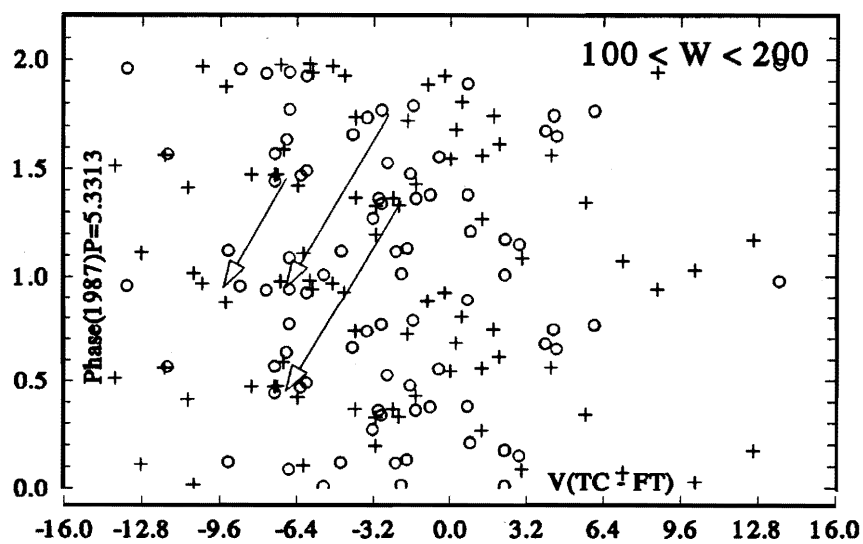

Fig 7. Phase-deviation diagram for TC − FT 300 foot telescope data on galaxies with profiles 100 to 200 km s^{-1} wide and S/N > 10. Open circles refer to symmetric profile objects and crosses refer to positively asymmetric objects. Phase is calculated for the 5.3313 km s^{-1} period epoch 1987 and plotted as a double cycle. The deviation scale is in km s^{-1}. The vectors illustrate tracks points would follow if undergoing a transition between levels. Each vector begins and ends at a concentration of points.

we find that the phase clumps are not randomly located; they associate as expected in the level and transition model. The intervals along the deviation axis were set at 2.6657 km s^{-1} before scaling for the epoch change. The vertical phase scale is set by the predetermined 5.3313 km s^{-1} periodicity and is independent of epoch. The phase changes which occurs for the transitions shown in Figure 7 are not obviously simply related to the period. The size of the phase change depends upon the choice of epoch, however. We will reconsider this point in section 6.

To demonstrate the periodicity more explicitly the data in Figure 7 are replotted in Figure 8 at the 2.6657 km s^{-1} period. Since we have no a prori means of predicting the phase at which maximum clumping occurs, we will discuss the clumping using the free-phase In/Out ratio technique from Tifft and Cocke (1984). Only two of the 32 points negative of deviations -4.8 km s^{-1}, which contains the principal clumps at -6.4 km s^{-1} and more deviant points, fall outside a half phase interval. Such a 16:1 concentration ratio for 32 points has a liklihood of random occurrence of less than 0.0001. There can be little doubt that the galaxies in the large negative deviation wing of the FT data are periodically distributed in redshift at the predetermined 2.6657 km s^{-1} period. We will reconsider the periodicity over a broader range of deviations in section 6.

As discussed and demonstrated in section 4, we have reason to expect asymmetry to distinguish between subsamples within a profile width interval. Restricting the asymmetry range for the narrow profile objects appeared to separate subgroups in a manner consistent with the level and transition model. We find the same situation applies to the intermediate width profile sample. Figure 9 shows the P = 5.3313 km s^{-1} phase-deviation diagram for the A < -1.04 galaxies omitted in the previous discussion. The extreme positive, A > 1.04, galaxies are also shown, as are two of the transition vectors. The symmetric profile objects, which match the positive asymmetry objects very closely, are omitted for clarity. The transition vector omitted is defined almost entirely by symmetric profile objects. The negative A galaxies are seen to fall systematically below the positive A objects for all the significant clumps. They lie along transition vectors in advance of positive points as found for the narrow profiles. A phase shift of about 0.15 will superimpose the negative points quite precisely on the positive ones. The intermediate width profile data appear to be completely consistent with the narrow profile findings and the level and transition model.

The positive-negative offset in Figure 9 may provide some additional information. We presume that some underlying mechanism is producing the periodicities and apparent changes we see. The phenomenon is manifest through the redshift which is estimated by means of a specific measurement algorithm. The asymmetry offset in Figure 9 will include any failure of the measurement to accurately represent the underlying mechanism. The agreement of the symmetric and positive profile objects, and the small size of the negative

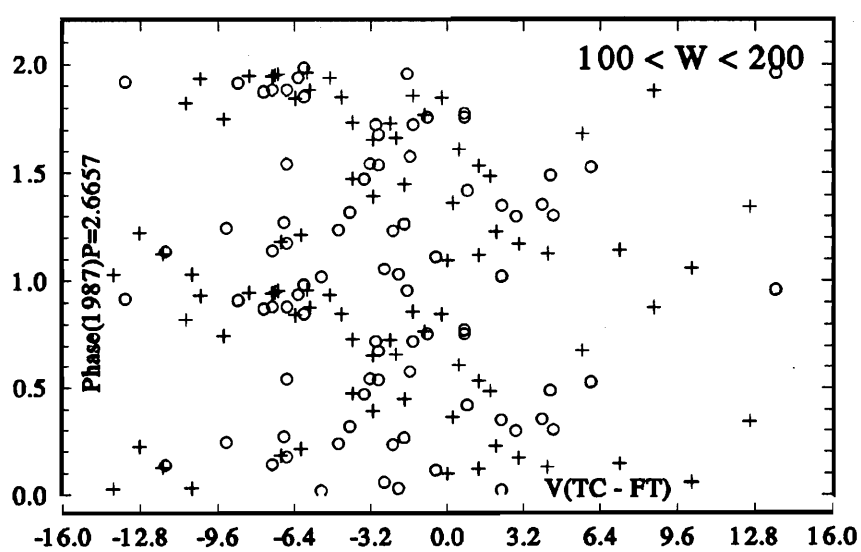

Fig 8. Phase-deviation diagram for TC − FT 300 foot telescope data on galaxies with profiles 100 to 200 km s^{-1} wide and S/N > 10. Symbols are the same as in figure 7. Phase is calculated for the 2.6657 km s^{-1} period epoch 1987 and plotted as a double cycle. The deviation scale is in km s^{-1}. A strong periodicity for objects with large negative deviations is present.

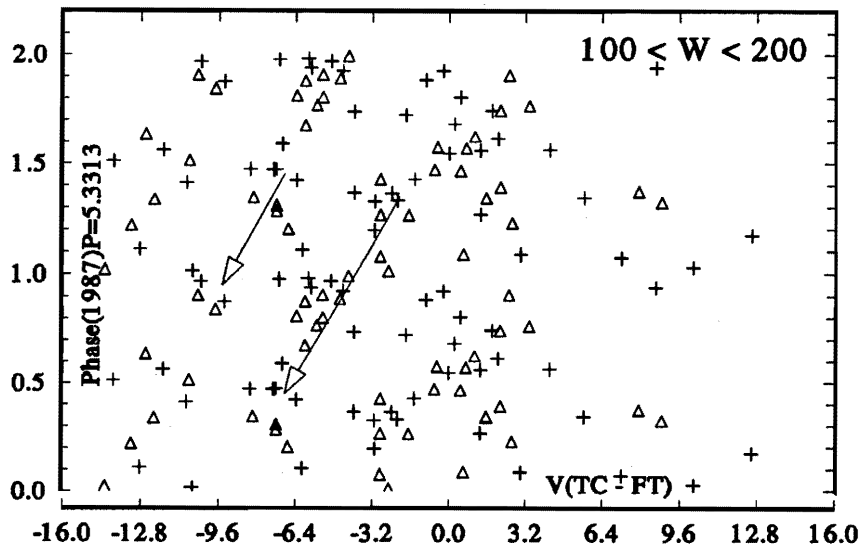

Fig 9. Phase-deviation diagram for TC − FT 300 foot telescope data on galaxies with profiles 100 to 200 km s^{-1} wide and S/N > 10. Crosses refer to positively asymmetric profile objects and triangles to negative ones. Phase is calculated for the 5.3313 km s^{-1} period at epoch 1987 and plotted as a double cycle. The deviation scale is in km s^{-1}. Two transition vectors are copied from figure 7. The negatively asymmetric objects are systematically shifted from positive objects in the transition direction.

offset, suggest that any systematic representation errors must be small. The fact that the negative, but not the positive, profiles are shifted with respect to symmetric ones suggests that it is not the asymmetry itself which produces the offset. Regardless of the interpretation, asymmetry does appear to distinguish subsamples in a consistent manner.

6. THE STANDARDS IN OCTOBER 1991

Solar interference disturbs baselines, especially at the wider bandwidths. The October 1991 140 foot telescope observations permitted observations of wide profile galaxies located near the Sun in May and afforded an opportunity to reobserve nearly all the standards. As discussed in sections 4 and 5, the model which appears to fit the TC and FT redshift data best is one where relatively stable discreet levels are occupied for some time, followed by a brief period of transition to a different, generally lower, level. The May 1991 observations, discussed in section 3, show the appropriate periodicity but a phase gradient rather than simple displaced levels. As noted in section 5, such a gradient might occur if some objects were in the process of changing levels in May. The October observations provide an opportunity to test this idea. On the basis of the discussion in the previous sections we would expect to see a negatively displaced wing begin to develop. Concentrations of points near at least the first multiple of 2.6657 km s^{-1} should probably develop. Three or more such states seem to have appeared during the 10-12 years between the FT and TC observations; a typical time scale of about three or four years is suggested. The 1991 observations occurred three years after the establishment of the standards; consistency would suggest that deviations should begin to develop.

In Figure 10 we display the distribution of redshift deviations between the two 1991 data sets and the 1988 standard values. The galaxies are separated by profile width, which also separates them fairly closely by the bandwidth used in the observations. A few points with S/N of 8 or 9 are shown as open circles, otherwise S/N is 10 or greater. Table 3 summarizes the results of the comparisons. The table contains the mean deviation, with its mean error, and the dispersion for each range of profile width and S/N indicated in Figure 10. The number of objects in each sample is given; a few cases with discordant points are noted.

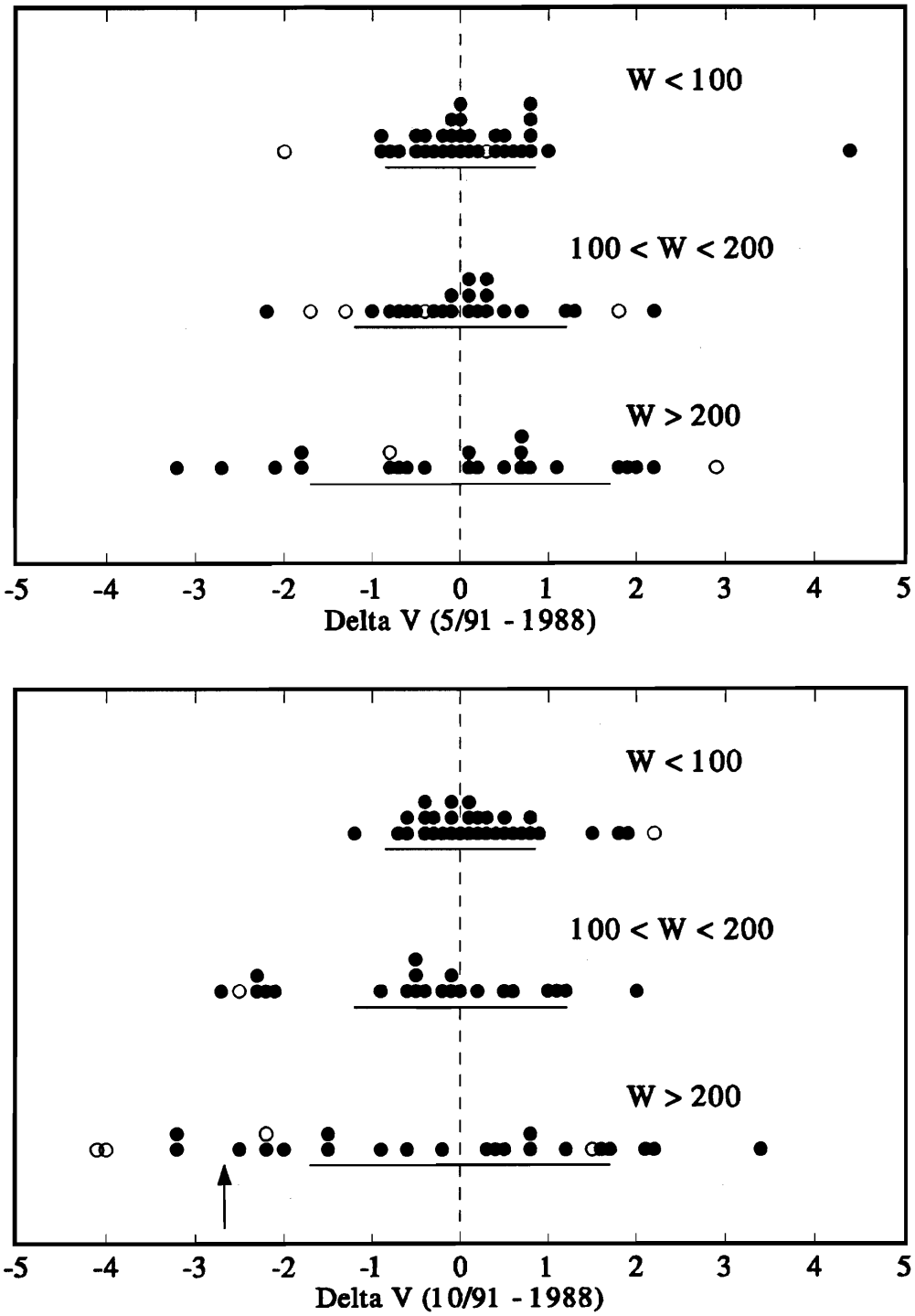

Fig 10. Residuals for 1991 redshift observations of the 21 cm standards established in 1988. The upper panel contains data from May, the lower from October. Open circles refer to data with S/N < 10. The data are separated by profile width and approximately by bandwidth. The line beneath each distribution illustrates the typical uncertainty previously determined for intersystem comparisons. The line extends $\pm$ 1σ. The actual scatter in May was less by a factor 1.4. The October data show a negative deviation for the wider profile data; the mark on the deviation scale at -2.6657 km s^{-1} indicates where the first displaced state is predicted to concentrate.

Table 3

Redshift Comparisons, 1991 – 1988

N	Run	W km s^{-1}	S/N	ΔV±mem km s^{-1}	σ km s^{-1}	Reject
32	May	<100	≥10	0.05±0.10	0.53	1>3σ
34	May	<100	≥9	−0.00±0.11	0.63	1>3σ
22	May	100-200	≥10	0.04±0.20	0.89	
26	May	100-200	≥8	−0.03±0.20	0.99	
22	May	>200	≥10	−0.06±0.34	1.53	1>3σ
24	May	>200	≥8	0.03±0.34	1.59	1>3σ
33	Oct	<100	≥10	0.18±0.12	0.70	1>3σ
34	Oct	<100	≥9	0.24±0.14	0.77	1>3σ
22	Oct	100-200	≥10	−0.40±0.28	1.27	
23	Oct	100-200	≥9	−0.49±0.29	1.32	
21	Oct	>200	≥10	−0.13±0.43	1.88	1>3σ
25	Oct	>200	≥9	−0.46±0.44	2.09	1>3σ

Random error analysis in TH and Paper I indicated typical redshift uncertainties, for S/N > 10, of 0.6 km s^{-1} at a bandwidth 2.5 MHz; the uncertainty varies as the square root of the bandwidth. A horizontal line under each distribution in Figure 10 gives the predicted 1 sigma scatter for redshift differences if these rules apply. These are respectively 0.85, 1.2 and 1.7 km s^{-1}. The May 1991 comparisons indicate that the actual scatter is about a factor 1.4 less. Furthermore, some of the spread arises through the non-random phase dependent correlations. The TH and Paper I estimates of uncertainty include intersystem and resolution dependent effects which may partially explain the difference. The differential internal consistency of the 140 foot data is clearly underestimated if we use the TH and Paper I values. For the purpose of discussion we will assume rms uncertainties in the 1991 data are 0.6, 0.85, and 1.2 km s^{-1} for the three deviation distributions. The data in Table 3 also show that systematic deviations in May 1991 were zero. There can be very little doubt that precise sub km s^{-1} comparisons are possible using such data.

The lower panel of Figure 10 contains the October 1991 deviation distribution. The intermediate and wide profile data are noticeably shifted toward negative deviations. A marker is shown at −2.6657 km s^{-1} where we have reason to expect points to concentrate if our initial assessments of redshift time dependence are correct; the data are consistent with this expectation. Table 3 shows that the scatter in the October data is greater than it appeared to be in May. This would also be expected if a real shift occurred. Since we have reason to expect deviations we have reason to question the validity of the October error estimates. The quality of the data from both runs is excellent; the average signal-to-noise level is, if anything, slightly higher for the October data. Whereas the May deviation distributions are adequately fit with normal error distributions this is not the case in October. A normal error distribution has only one point in 20 beyond 2σ. If the rms uncertainties discussed for the May data apply, then the intermediate width group in October has 6 or 7, and the wide profile group has 5 or 6. In both cases the excess is on the negative side as we would expect. The mean deviation of the intermediate profile galaxies is at or beyond the 2σ point if the mean error of the mean from May is a proper measure of the mean uncertainty. A possible positive deviation for the narrow profiles will be briefly discussed in section 7.

If the negative displacement in the intermediate width profile galaxy redshifts is real, the level and

transition model requires the objects to be in phase or related along a transition line. Figure 11 shows that this is the case, four of the five points with S/N > 10 are closely grouped in phase. The October 1991 phase-deviation pattern is shown superimposed on the TC−FT diagram from Figure 9 advanced to epoch 1988.25. We see that not only are the displaced points in 1991 grouped in phase, they are generally in phase with the transformation of the older data. Although the variation of epoch by a year or two will not change the phase agreement much, the transformation of the older data to an epoch in 1988 produces a pattern of levels with rather special properties. Whereas the transition intervals in Figures 7 or 9 are not simple fractions of the period, they are at the 1988 epoch. The pattern of levels is a simple staggered pattern of 2.6657 km s^{-1} clumps; the 1991 phase agreement places the new data within the same pattern.

Whereas the transformation of the TC−FT data to epoch 1987 aligns the scatter generally horizontally in the main groups, the 1988 epoch aligns the groups themselves. In the 1988 alignment the 2.6657 km s^{-1} periodicity is easily demonstrated across the entire range of deviations. The half-phase In/Out concentration ratio is 3.7 for 42 positively asymmetric objects and 2.4 for 84 objects if we include the symmetric profile galaxies. The free-phase likelihoods of such concentrations occuring by accident are 0.005 and 0.003. Although we have some orientation flexibility and asymmetry restrictions the level and transition model provides guidelines which limit the choices considerably. A very high level of consistency exists throughout the TC, FT and new 140 foot telescope data.

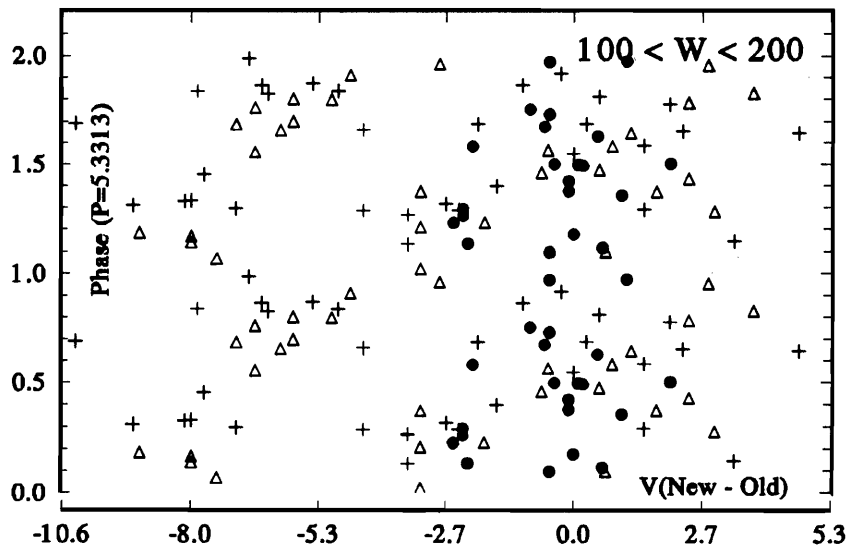

Fig 11. Phase-deviation diagram for the October 1991 140 foot observations (filled circles), superimposed on TC − FT 300 foot telescope data for galaxies with profiles 100 to 200 km s^{-1} wide and S/N > 10. The 300 foot data and symbols are identical to figure 9 except the epoch has been advanced to 1988.25. At his epoch the TC − FT deviations form a simple staggered pattern of displaced clumps spaced at multiples of 2.6657 km s^{-1}. The deviant points from the new October 1991 data are grouped in phase and suggest that a new group, consistent with the older ones, is in the process of forming. The 140 foot data is plotted at epoch 1991.

7. SUMMARY AND DISCUSSION

The TC study in the mid 1980s marked the begining of a series of 21 cm observations which now extends over 7 years. The original objective of determining uncertainties and providing a set of precision redshifts was largely acomplished by the TC study and the TH and Paper I work which followed in 1987-88. The program might have ended then except for unexpected discrepancies in global phase patterns found when comparing TC and FT global periodicity studies. Deviations appeared to correlate with global redshift phase in a manner which ordinary random or systematic error could not explain. The possibility that the redshift might be varying significantly over periods of only a few years was presented in 1987 (Tifft, 1988);

confirmation testing using an entirely internal time baseline from 300 foot telescope data followed in 1989 (Tifft & Cocke 1990). The basis for redshift time variability was subsequently examined in detail in Paper III where the phase-deviation diagram was developed as a tool for tracking redshift changes and fine tuning global redshift parameters and the short global periodicities involved. The loss of the 300 foot telescope in 1988 prevented extending the time baseline of the large TC sample and its 1988 extensions; however, the establishment of the standards in 1988, including the 140 foot telescope, assures that basic monitoring can continue into the 90s until the Green Bank Telescope (GBT) is available. The GBT can provide a link back to TC equivalent in time baseline to TC back to FT, but with much enhanced precision. The time dependent redshift model set forth in this paper is a first attempt to provide a model suitable to guide the future course of work.

The 140 foot second epoch observations of the standards in 1991 provided a three year time baseline, sufficient to confirm that redshift phase appears to correlate with the differences in redshift between 1988 and 1991. The periods at which the correlations appear are multiples of the 2.6657 km s^{-1} period recognized in Paper III. Subsequent reanalysis of the narrow profile 300 foot data, comparing TC and FT redshifts and distinguishing samples by profile asymmetry, has permitted refining the time drift concepts of Paper III into a level and transition model with predictive power. This model has provided the basis for a detailed analysis of intermediate width profile galaxies where we have found consistent results. A second test, using the latest 140 foot observations appears to indicate that the same patterns seen in the TC to FT comparisons are now developing in the new data.

The level and transition model views the redshift as occurring in specific relatively stable levels spaced at intervals of 2.6657 km s^{-1}. During relatively brief periods, spaced several years apart, transitions bridging one, or perhaps several, levels occur. The population within the levels appears to be modulated over a range of levels giving rise to various longer periodicities. The frequency and/or times of transition appear to differ between levels and generate larger scale patterns. Profile shape is a factor relating to the timing of transitions; negatively asymmetric profile objects tend to precede. Galaxies showing positive deviations, redshifts increasing in time, appear to be fewer in number, the dominant direction of change being down in redshift. Over time a negative deviation wing develops in the redshift residuals. The deviation seems to develop faster for wider profiles; the negative wing is less prominent for narrow profile data. Narrow and intermediate width profiles are separated by a transition region, W= 75-100 km s^{-1}, where properties appear to change.

In addition to the width dependence the character of phase-deviation diagrams changes in passing from negative to positive deviations. A phase shift typically occurs at zero deviation. There is some indication that brief positive deviations may precede a negative shift. Such a positive deviation may be present in the narrow profile data from October 1991. The current analysis is limited to galaxies with profiles less than 200 km s^{-1} wide. The amount and precision of data on wider profiles is insufficient for a detailed investigation although similar trends are present.

On the basis of the model as now formulated, we can predict that continued monitoring will show the progressive development of a negative deviation wing. For narrow and intermediate width profile galaxies the wing will presumably contain displaced levels periodic in multiples of 2.6657 km s^{-1}. A related but slightly different period is suspected to apply to wide profile objects. A series of regular observations will be required to determine if levels are actually stable. By the mid 1990s we would expect several displaced levels to exist. The small size and large beam of the 140 foot telescope limits the choice and number of objects being monitored to a few hundred. The 100 standards are the primary objects being observed; however, a similar list emphasizing wider profile objects has been added. When the GBT becomes available in the mid 1990s the 300 foot telescope data can be closely duplicated; overlap with more than 1000 galaxies will be possible linking FT, TC, and the GBT in a time sequence spanning 20 years. A definitive test of redshift time variability should be possible within a few years. There is some evidence that profile shape and total flux also vary. Future monitoring will address these questions as well.

The importance of resolving the question of time dependence in the redshift requires little debate. Aside from obvious implications relating to mass calculations and dark matter, an entirely new class of explanations may apply to various large scale phenomena. Several examples are illustrative. If different morphologies change at different rates or times we will observe morphological separations in redshift within individual aggregates of galaxies; such separations have been reported in clusters and among general field galaxies. One

interesting example concerns the excess redshift of dwarf galaxies in small groups reported originally by Arp (see Arp & Sulentic 1985). We have seen in Paper III and this paper that the narrow profile dwarf galaxies appear to drift more slowly toward lower redshifts than the wider profile luminous galaxies; over time a net higher redshift for the dwarf galaxies in a group would be a natural consequence of this process. Although the rates of drift appear to be extraordinarily large there is good reason for believing that over long periods the differential deviations that develop must be limited. If this were not the case clusters and groups would be unrecognizable. The range of redshift in clusters and groups may provide a means of estimating the amplitude of redshift oscillations.

One of the principal difficulties in interpreting redshift-magnitude bands and morphological correlations in clusters was the apparent requirement for rapid evolution. Rapid redshift variability, along with luminosity and morphological evolution, was proposed (Tifft 1979). If the redshift variation proposed in this paper is confirmed then such models may have to be reexamined. The use of apparent large scale motion as a probe of the large scale matter distribution may be questionable as may be the interpretation of some of the large scale structure itself. If certain classes of objects evolve in redshift very slowly, number counts as a function of redshift may not reflect number or density evolution in the normal manner. It is obvious that numerous conclusions and discrepancies on the large scale relate very intimately to our understanding of the redshift phenomenon. A very critical fundamental test of the nature of the redshift is now avilable to us.

REFERENCES

Arp, H. & Sulentic, J. W., 1985, ApJ, 291, 88

Fisher, J. R., & Tully, R. B., 1981, ApJS, 47, 139 (FT)

Nilson, P., 1973, **Uppsala General Catalog of Galaxies** (*Nova Acta Reg. Soc. Upsaliensis.* Ser. V:A., Vol. 1)

Tifft, W. G., 1979, ApJ, 233, 799

Tifft, W. G., 1988, **New Ideas in Astron.** ed. F. Bertola, J. Sulentic, B. Madore, (Cambridge:Cambridge), pg 173

Tifft, W. G., 1990, ApJS, 73, 603 (Paper I)

Tifft, W. G., 1991a, ApJ, 368, 105 (Paper II)

Tifft, W. G., 1991b, ApJ, 382, 396 (Paper III)

Tifft, W. G., 1992, ApJS, in press Feb. (Paper IV)

Tifft, W. G., & Cocke, W. J., 1984, ApJ, 287, 492

Tifft, W. G., & Cocke, W. J., 1988, ApJS, 67, 1 (TC)

Tifft, W. G., & Cocke, W. J., 1990, IAU Colloq. 124, **Paired and Interacting Galaxies**, ed. J. Sulentic, W. Keel, C. Telesco, (NASA Conf. Publ. 3098), pg 479

Tifft, W. G., & Huchtmeier, W. K., 1990, A&AS, 84, 47 (TH)